arXiv:1512.04261v1 [physics.chem-ph] 14 Dec 2015

Analysis of electrolyte transport through charged nanopores

P.B. Peters,[1,2] R. van Roij,[1] M.Z. Bazant,[3,4] and P.M. Biesheuvel[5,6]

[1]Institute for Theoretical Physics, Center for Extreme Matter and Emergent Phenomena, Utrecht University, Leuvenlaan 4, 3584 CE Utrecht, The Netherlands.
[2]Fitzwilliam College, Cambridge University, Cambridge CB3 0DG, United Kingdom.
[3]Department of Chemical Engineering, Massachusetts Institute of Technology, Cambridge, MA 02139, USA.
[4]Department of Mathematics, Massachusetts Institute of Technology, Cambridge, MA 02139, USA.
[5]Wetsus, European Centre of Excellence for Sustainable Water Technology, Oostergoweg 9, 8911 MA Leeuwarden, The Netherlands.
[6]Laboratory of Physical Chemistry and Soft Matter, Wageningen University, Dreijenplein 6, 6703 HB Wageningen, The Netherlands.

Abstract

We revisit the classical problem of the flow of an electrolyte solution through charged capillaries (nanopores). In the limit where the length of the capillary is much larger than its radius, the problem can be simplified to a one-dimensional averaged flux-force formalism that relates the relevant fluxes (electrical current, salt flux, fluid velocity) to their respective driving forces (difference in electric potential, salt concentration, pressure). Calculations in literature mainly consider the limit of non-overlapping electrical double layers (EDLs) in the pores and the absence of salt concentration gradients in the axial direction. In the present work these simplifications are relaxed and we discuss the general case with overlapping EDLs and nonzero axial salt concentration gradients. The 3×3 matrix that relates these quantities exhibits Onsager symmetry and for one of the cross coefficients we report a new significant simplification. We describe how Onsager symmetry is preserved under change of variables which we illustrate by one example of a different flux-force matrix given by Gross and Osterle (1968). The model is well-suited to physically represent membranes consisting of charged nanopores for electrokinetic energy conversion and water desalination. We analyse the energy conversion of a salt concentration difference into electrical power using an efficiency vs. power diagram. Because of the non-zero axial gradient in salt concentration that we allow in our calculations, under wide ranges of conditions, partial loops in current, salt flux or fluid flow are predicted in the pore.

1 Introduction

Charged capillary nanopores are found in many natural and technological systems, as part of porous membranes separating two aqueous electrolytes [1–8]. Membranes containing charged nanopores can be used for water desalination, selective ion removal, and electrokinetic energy conversion. In the steady-state, transport is defined by three fluxes (salt flux, electrical current, fluid velocity) and three driving forces (salt concentration difference, electric potential difference, pressure difference). In any physical situation, three out of these six fluxes or forces are required (prescribed) to fully define the problem, with the other three physical quantities to be measured or calculated. It is also possible that one of the three defining relations includes a combination of factors, such as a relation between current and electric potential difference (i.e., applying a constant external load).

The theory for charged capillaries dates back to the work of Osterle and coworkers [2,3] and describes the flow of ions and water through a cylindrical pore carrying a homogeneous charge on its inner surface. The ions are assumed to be monovalent point charges. The pore is connected to two reservoirs that can be different in salt concentration, pressure and/or electric potential. The length L of the pore is assumed to be much larger than the pore radius R. The physical situation is illustrated in Fig. 1.

In this work we revisit the Osterle-framework [2,3] for flow through charged capillaries (also used by Sasidhar and Ruckenstein [4]) and show how one crucial three-fold integral across the pore radius can be simplified to a single integral, thereby significantly simplifying the numerical calculations. We will demonstrate how an infinite number of local flux-force relationships are in principle possible, all abiding Onsager symmetry.

While much theoretical literature only considers situations without overlap of the electrical double layers (EDLs) in the pores and neglects axial salt concentration gradients, we will consider the most general case including EDL overlap and axial salt gradients. Note that even when two external bulk solutions may have an equal salt concentration, because of concentration polarization at both membrane interfaces (described by the concept of the Nernst diffusion boundary layer [9]), at the entrance of the pores the salt concentration can yet be very different, requiring the general approach as we will discuss.

We provide numerical results for electrokinetic energy conversion, and in-pore current profiles, for pores with EDL overlap in the presence of an overall salt concentration difference. Though we present only calculation results for the steady-state, the model can be extended quite straightforwardly to dynamic situations.

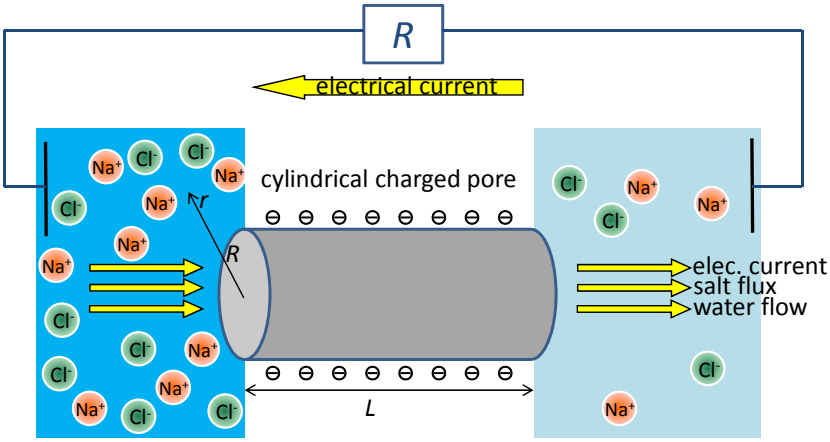

Figure 1: Sketch of a charged cylindrical pore subjected to water flow, electrical current and salt flux between a high salinity (left) and low-salinity (right) reservoir.

2 General theory

2.1 Governing equations

The derivation that follows closely resembles that of Gross and Osterle [2], Fair and Osterle [3] and Sashidar and Ruckenstein [4]. Central to the theory are three equations: the extended Navier-Stokes (NS) equation, the extended Nernst-Planck (NP) equation and the Poisson-Boltzmann (PB) equation. The NP-equation describes the molar flux $\boldsymbol{J}_i$ (mol/m^2/s) of ions of species i by

$$\boldsymbol{J}_i(x,r) = c_i(x,r)\boldsymbol{u}(x,r) - D_i\left(\nabla c_i(x,r) + \frac{z_i c_i}{\Phi_B}\nabla\Phi(x,r)\right) \tag{1}$$

where $c_i(x,r)$ is the local ion concentration (mM=mol/m^3), $\Phi(x,r)$ the local electrical potential (V), Φ_B the thermal voltage ($= R_gT/F$), and D_i is the diffusion coefficient of species i (m^2/s) with $i \in \{+,-\}$. The ion valency z_i is either $+1$ or -1 because we will consider only a 1:1 salt (with ions, e.g., Na^+ and Cl^-). Further, $\boldsymbol{u}$ is the velocity of the fluid (m/s) and T temperature (K). The Faraday constant is $F = 96485$ C/mol and the ideal gas constant is $R_g = 8.3144$ J/mol/K. Eq. (1) assumes that ions are volumeless point charges.

In this work we will consider a stationary state and thus the ion mass balance

$$\frac{\partial c_i(x,r)}{\partial t} + \nabla\cdot\boldsymbol{J}_i(x,r) = 0 \tag{2}$$

simplifies to $\nabla\cdot\boldsymbol{J}_i(x,r) = 0$. Throughout we assume cylindrical symmetry, see Fig. 1, with the axial coordinate $x \in [0,L]$ and the radial coordinate $r \in [0,R]$.

For laminar flow, fluid flow is described by the NS-equation, which at the low Reynolds number of interest here is given by

$$\mu\nabla^2\boldsymbol{u}(x,r) - \nabla p_h(x,r) - \rho(x,r)\nabla\Phi(x,r) = 0 \tag{3}$$

where μ is viscosity (Pa.s), $p_h(x,r)$ hydrostatic pressure (Pa), and $\rho(x,r)$ the local charge density (C/m^3).

Finally, Poisson's equation relates the potential $\Phi(x,r)$ to the charge density as

$$\nabla^2\Phi(x,r) = -\frac{\rho(x,r)}{\varepsilon} = -\frac{F}{\varepsilon}(c_+(x,r) - c_-(x,r)) \tag{4}$$

where ε is the permittivity of the medium (F/m). In the second equality we implement the assumption of a 1:1 salt (both ions monovalent).

2.2 Boundary conditions & further assumptions

Because the pore is much longer than wide, we can assume local equilibrium in r-direction and decompose the total potential as

$$\Phi(x,r) = \phi(x) + \psi(x,r) \tag{5}$$

where $\psi(x,r)$ is obtained from an equilibrium PB-model, and $\phi(x)$ accounts for axial gradients in potential (along the length of the pore). Concerning the fluxes $\boldsymbol{J}_i$ and $\boldsymbol{u}$, the walls of the pore are impermeable to the both the fluid and the ions, so we have

$$J_{i,r}(x,R) = 0 \quad \text{and} \quad u_r(x,R) = 0 \tag{6}$$

where the subscript r denotes the radial component of the vector quantities $\boldsymbol{J}_i(x,r)$ and $\boldsymbol{u}(x,r)$. We also assume no-slip boundary conditions for the fluid velocity $\boldsymbol{u}$, i.e.,

$$u_x(x,R) = 0 \tag{7}$$

where we stress that this does not hold for the ion fluxes $\boldsymbol{J}_i$.

Naturally, the system we have described is out of equilibrium and to account for this, "virtual" quantities are defined. A physical quantity $F_v(x)$ (subscript "v") is defined as "virtual" when it represents conditions in a virtual reservoir that is in equilibrium with any differential volume ("slice") in the pore. Thus, it represents conditions under which a cylindrical pore cross-section, or slice, is in equilibrium with a charge neutral reference volume. From this definition it follows that virtual quantities will be x-dependent only. Common virtual quantities that we will encounter are the virtual concentration $c_v(x)$, virtual pressure $p_{t,v}(x)$ and virtual potential $\phi_v(x)$. With this formalism defined, we can impose the most important assumption, namely that the length of the cylinder is much larger than its radius ($L \gg R$). We are then allowed to consider the solution inside this thin pore to be in equilibrium in the radial direction [10] leading to

$$J_{i,r}(x,r) = 0 \quad \text{and} \quad u_r(x,r) = 0 \tag{8}$$

allowing us to derive a radial PB-equation by inserting Eqs. (5) and (8) in the r-component of Eq. (1) which results in

$$\frac{\partial c_i(x,r)}{\partial r} = -\frac{z_i c_i(x,r)}{\Phi_B}\frac{\partial\psi(x,r)}{\partial r} \tag{9}$$

which can be integrated to

$$c_i(x,r) = c_v(x)\exp\left(-z_i\frac{\psi(x,r)}{\Phi_B}\right) \tag{10}$$

which is a Boltzmann distribution with $c_v(x)$ a yet undetermined integration constant. Implementing Eq. (10) in Eq. (4) we obtain the desired PB-equation,

$$\nabla^2\Phi(x,r) = 2\frac{Fc_v(x)}{\varepsilon}\sinh\left(\frac{\psi(x,r)}{\Phi_B}\right) \tag{11}$$

which will be solved with the boundary conditions (using cylindrical symmetry)

$$\left.\frac{\partial\psi(x,r)}{\partial r}\right|_{r=R} = +\frac{\sigma}{\varepsilon} \quad \text{and} \quad \left.\frac{\partial\psi(x,r)}{\partial r}\right|_{r=0} = 0 \tag{12}$$

where σ denotes the surface charge density of the pore wall (in C/m^2).

2.3 Non-dimensional formulation

In order to simplify our governing equations (1), (3) and (11) it is convenient to non-dimensionalize all our equations and physical quantities by dividing them with an appropriate reference quantity. This change of variables is listed below and with a slight abuse of notation we replace all variables by their dimensionless counterparts, as follows,

$$\begin{aligned}
\frac{r}{R} &\to r & \frac{x}{L} &\to x \\
\frac{\phi_v(x)}{\Phi_B} \to \phi_v(x), \frac{\psi(x,r)}{\Phi_B} &\to \psi(x,r) & \Phi_B &= \frac{R_g T}{F} \\
\frac{c_v(x)}{c_{\text{ref}}} &\to c_v(x) & c_{\text{ref}} &= \frac{\mu D}{R_g T R^2} \\
\frac{\boldsymbol{J}_i(x,r)}{J_{\text{ref}}} &\to \boldsymbol{j}_i(x,r) & J_{\text{ref}} &= \frac{D c_{\text{ref}}}{L} \\
\frac{\boldsymbol{u}(x,r)}{u_{\text{ref}}} &\to \boldsymbol{u}(x,r) & u_{\text{ref}} &= \frac{D}{L} \\
\frac{p_h(x,r)}{p_{\text{ref}}} &\to p_h(x,r) & p_{\text{ref}} &= c_{\text{ref}} R_g T \\
\frac{\sigma}{\sigma_{\text{ref}}} &\to \sigma & \sigma_{\text{ref}} &= \frac{\varepsilon \Phi_B}{R}
\end{aligned} \tag{13}$$

where D is the (assumed equal) diffusion coefficient of both types of ions. With this change of variables we now have $r \in [0,1]$ and $x \in [0,1]$. Like the hydrostatic pressure, p_h, other pressures to be introduced below are also dimensionless, with reference pressure p_{ref}. From this point onward, all equations and parameters will be non-dimensional, unless otherwise stated.

Next we proceed with the approximation that in the limit $L \gg R$, we can ignore the $\frac{\partial^2}{\partial x^2}$ terms in both the NS-equation (3) and PB-equation (11), which is a well-known procedure [10]. Eq. (11) can now be written as

$$\frac{1}{r}\frac{\partial}{\partial r}\left(r\frac{\partial \psi(x,r)}{\partial r}\right) = \frac{c_v(x)}{\lambda_{\text{ref}}^2}\sinh\psi(x,r) \tag{14}$$

where

$$\lambda_{\text{ref}} = \sqrt{\frac{\varepsilon \Phi_B}{2F c_{\text{ref}} R^2}} = \sqrt{\frac{\varepsilon \Phi_B^2}{2\mu D}} \tag{15}$$

is a dimensionless reference Debye length. The boundary conditions to the PB-equation become

$$\left.\frac{\partial \psi(x,r)}{\partial r}\right|_{r=1} = +\sigma \quad \text{and} \quad \left.\frac{\partial \psi(x,r)}{\partial r}\right|_{r=0} = 0 \tag{16}$$

while the Boltzmann distribution of Eq. (10) is now written as

$$c_i(x,r) = c_v(x)\exp(-z_i\psi(x,r)). \tag{17}$$

Performing the change of variables in Eq. (13) we can also simplify the NP-equation in x-direction (which currently is the only direction of interest for the ion fluxes), resulting in

$$j_{i,x}(x,r) = c_i(x,r)u_x(x,r) - \frac{\partial c_i(x,r)}{\partial x} - z_i c_i(x,r)\frac{\partial(\psi(x,r)+\phi_v(x))}{\partial x}. \tag{18}$$

Finally, we can also simplify the NS-equation by ignoring the $\frac{\partial^2}{\partial x^2}$ terms and substituting Eq. (13). In the x-direction we find that

$$\frac{1}{r}\frac{\partial}{\partial r}\left(r\frac{\partial u_x(x,r)}{\partial r}\right) - \frac{\partial p_h(x,r)}{\partial x} + 2c_v(x)\sinh\psi(x,r)\frac{\partial(\psi(x,r)+\phi_v(x))}{\partial x} = 0. \tag{19}$$

3 Radially averaged flux-force relationships

In a next step, mathematical expressions are derived for radially averaged fluxes, which in the case of a flux component $f(x,r)$ take the form of

$$\overline{f(x)} = 2\int_0^1 r \cdot f(x,r)dr. \tag{20}$$

Our aim will be to derive Onsager relations between the x-component of the averaged fluxes $\overline{u_x(x)}$, $\overline{j_{\text{ions},x}(x)}$ and $\overline{j_{\text{charge},x}(x)}$, and the driving forces $-\partial_x p_{t,v}(x)$, $-\partial_x \mu_v(x)$ and $-\partial_x \phi_v(x)$. Here, the ion flux $\boldsymbol{j}_{\text{ions}}$ and ionic current $\boldsymbol{j}_{\text{charge}}$ are defined as

$$\begin{aligned} \boldsymbol{j}_{\text{ions}}(x,r) &= \boldsymbol{j}_+(x,r) + \boldsymbol{j}_-(x,r) \\ \boldsymbol{j}_{\text{charge}}(x,r) &= \boldsymbol{j}_+(x,r) - \boldsymbol{j}_-(x,r). \end{aligned} \tag{21}$$

Furthermore, the virtual chemical potential, $\mu_v(x)$, virtual osmotic pressure, $\pi_v(x)$, and virtual total pressure, $p_{t,v}(x)$, are defined as

$$\begin{aligned} \mu_v(x) &= \ln c_v(x) \\ \pi_v(x) &= 2c_v(x) \\ p_{t,v}(x) &= p_{h,v}(x) - \pi_v(x). \end{aligned} \tag{22}$$

To simplify the notation, from this point onward, the x-dependencies of the various quantities will no longer be explicitly stated. Inserting the NP-equation (18) and the Boltzmann distribution (17) into Eqs. (21), while also using the definitions of Eqs. (22), we immediately obtain an explicit expression for the ion flux and ionic current in the x-direction, namely

$$\begin{aligned} j_{\text{ions},x}(r) &= 2c_v \cosh\psi(r) u_x(r) - 2c_v \cosh\psi(r)\frac{\partial \mu_v}{\partial x} + 2c_v \sinh\psi(r)\frac{\partial \phi_v}{\partial x} \\ j_{\text{charge},x}(r) &= -2c_v \sinh\psi(r) u_x(r) + 2c_v \sinh\psi(r)\frac{\partial \mu_v}{\partial x} - 2c_v \cosh\psi(r)\frac{\partial \phi_v}{\partial x}. \end{aligned} \tag{23}$$

We now proceed to find an expression for $u_x(r)$. To this end we note that in the r-direction the dimensionless NS-equation becomes (using Eq. (17) and $u_r(r) = 0$ in Eq. (8)),

$$\frac{\partial p_h(r)}{\partial r} = -\rho(r)\frac{\partial \psi(r)}{\partial r} = 2c_v \sinh\psi(r)\frac{\partial \psi(r)}{\partial r} = 2c_v \frac{\partial \cosh\psi(r)}{\partial r}. \tag{24}$$

This result can again be integrated, which results in

$$p_h(r) - p_{h,v} = 2c_v(\cosh\psi(r) - 1). \tag{25}$$

Now we observe that by Eq. (24), the equation

$$\frac{\partial p_h(r)}{\partial x} = \frac{\partial p_{t,v}}{\partial x} + 2c_v \cosh\psi(r)\frac{\partial \mu_v}{\partial x} + 2c_v \sinh\psi(r)\frac{\partial \psi(r)}{\partial x} \tag{26}$$

should hold. Substituting this result back into the NS-equation (19) for the x-direction, we arrive at

$$\frac{1}{r}\frac{\partial}{\partial r}\left(r\frac{\partial u_x(r)}{\partial r}\right) = \frac{\partial p_{t,v}}{\partial x} + 2c_v \cosh\psi(r)\frac{\partial c_v}{\partial x} - 2c_v \sinh\psi(r)\frac{\partial \phi_v}{\partial x}. \tag{27}$$

Using the fact that $\partial_r u_x(0) = 0$, multiplying both sides by r and integrating, we now find

$$\begin{aligned} r\frac{\partial u(r)}{\partial r} &= \int_0^r \frac{r'}{r'}\frac{\partial}{\partial r'}\left(r'\frac{\partial u}{\partial r'}\right)dr' \\ &= \frac{1}{2}r^2\frac{\partial p_{t,v}}{\partial x} + 2c_v\int_0^r r'\cosh\psi(r')dr'\frac{\partial \mu_v}{\partial x} - 2c_v\lambda_{\text{ref}} r\frac{\partial \psi(r)}{\partial r}\frac{\partial \phi_v}{\partial x} \end{aligned} \tag{28}$$

where we reduced the last term by virtue of the identity

$$2c_v\int_0^r r'\sinh\psi(r')dr' = 2c_v\lambda_{\text{ref}}\int_0^r \frac{\partial}{\partial r'}\left(r'\frac{\partial \psi(r')}{\partial r'}\right)dr' = 2c_v\lambda_{\text{ref}} r\frac{\partial \psi(r)}{\partial r} \tag{29}$$

in which we used the PB-equation (14). Finally, dividing both sides of Eq. (28) by r and using $u_x(1) = 0$ we obtain

$$\begin{aligned} u_x(r) = &- \int_r^1 \frac{\partial u(r')}{\partial r'} dr' = -\frac{1}{4}(1-r^2) \cdot \frac{\partial p_{t,v}}{\partial x} \\ &- 2c_v \int_r^1 \frac{1}{r_1} \int_0^{r_1} r_2 \cosh\psi(r_2) dr_2 dr_1 \frac{\partial \mu_v}{\partial x} - 2\lambda_{\mathrm{ref}}^2 (\psi(r) - \psi_{\mathrm{wall}}) \frac{\partial \phi_v}{\partial x} \end{aligned} \tag{30}$$

which is an explicit expression for $u_x(r)$. It is now a straightforward endeavor to insert $u_x(r)$ back into Eqs. (21) and take the average defined by Eq. (20). The final result (after grouping all terms) can be written as a matrix equation, relating the fluxes, $\overline{u_x}$, $\overline{j_{\mathrm{ions},x}}$ and $\overline{j_{\mathrm{charge},x}}$, and driving forces, $-\partial_x p_{t,v}$, $-\partial_x \mu_v$ and $-\partial_x \phi_v$, according to

$$\begin{pmatrix} \overline{u_x} \\ \overline{j_{\mathrm{ions},x}} \\ \overline{j_{\mathrm{charge},x}} \end{pmatrix} = \begin{pmatrix} L_{11} & L_{12} & L_{13} \\ L_{21} & L_{22} & L_{23} \\ L_{31} & L_{32} & L_{33} \end{pmatrix} \cdot \begin{pmatrix} -\frac{\partial p_{t,v}}{\partial x} \\ -\frac{\partial \mu_v}{\partial x} \\ -\frac{\partial \phi_v}{\partial x} \end{pmatrix}. \tag{31}$$

Here, the coefficients of this L-matrix are dependent on the x-coordinate only and are given by

$$\begin{aligned} L_{11} &= \frac{1}{8} \\ L_{12} &= 4c_v \int_0^1 r \int_r^1 \frac{1}{r_1} \int_0^{r_1} r_2 \cosh\psi(r_2) dr_2 dr_1 \\ L_{13} &= 4 \int_0^1 r \lambda_{\mathrm{ref}}^2 (\psi(r) - \psi_{\mathrm{wall}}) dr \\ L_{21} &= c_v \int_0^1 (r - r^3) \cosh\psi(r) dr \\ L_{22} &= 8c_v \int_0^1 r \cosh\psi(r) \left(c_v \int_r^1 \frac{1}{r_1} \int_0^{r_1} r_2 \cosh\psi(r_2) dr_2 dr_1 dr + \frac{1}{2} \right) dr \\ L_{23} &= 8c_v \int_0^1 r \left(\cosh\psi(r) \lambda_{\mathrm{ref}}^2 (\psi(r) - \psi_{\mathrm{wall}}) - \frac{1}{2} \sinh\psi(r) \right) dr \\ L_{31} &= -c_v \int_0^1 (r - r^3) \sinh\psi(r) dr \\ L_{32} &= -8c_v \int_0^1 r \sinh\psi(r) \left(c_v \int_r^1 \frac{1}{r_1} \int_0^{r_1} r_2 \cosh\psi(r_2) dr_2 dr_1 dr + \frac{1}{2} \right) dr \\ L_{33} &= -8c_v \int_0^1 r \left(\sinh\psi(r) \lambda_{\mathrm{ref}}^2 (\psi(r) - \psi_{\mathrm{wall}}) - \frac{1}{2} \cosh\psi(r) \right) dr. \end{aligned} \tag{32}$$

We note that (apart from notation) this set of expressions is completely equivalent to the set of equations for L_{ij} by Gross and Osterle [2]. In a next step, we are concerned with reducing the complexity of the L_{ij} coefficients in Eq. (32). This can be done first and foremost by reducing the triple integrals to single integrals in L_{12}, L_{22} and L_{32}. In the notation of Sasidhar and Ruckenstein [4] this implies a reduction of the k_1, k_3 and k_7 integrals, given by

$$k_1 = \int_0^1 r \int_r^1 \int_0^{r_1} \frac{r_2}{r_1} \cosh\psi(r_2) dr_2 dr_1 dr = \frac{1}{4} \int_0^1 r(1-r^2) \cosh\psi(r) dr \tag{33}$$

$$\begin{aligned} k_3 &= \int_0^1 r \sinh\psi(r) \int_r^1 \int_0^{r_1} \frac{r_2}{r_1} \cosh\psi(r_2) dr_2 dr_1 dr \\ &= -\int_0^1 r \cosh\psi(r) \lambda_v^2 (\psi(r) - \psi_{\mathrm{wall}}) dr \end{aligned} \tag{34}$$

$$\begin{aligned} k_7 &= \int_0^1 r \cosh\psi(r) \int_r^1 \int_0^{r_1} \frac{r_2}{r_1} \cosh\psi(r_2) dr_2 dr_1 dr \\ &= -2 \int_0^1 r \cosh\psi(r) \ln r \left(\frac{1}{2} r^2 \cosh\psi(r) - \left(\frac{\lambda_v}{2} r \frac{\partial \psi(r)}{\partial r} \right)^2 \right) dr. \end{aligned} \tag{35}$$

In the above equations the reduced form of k_7 to a single integral is a new result, and thus by substituting Eqs. (33)-(35) into Eq. (32), we can now show for the first time that all L_{ij} expressions can be reduced to single integrals only. Computationally this had the advantage of being able to formulate all the L_{ij} coefficients in terms of a first order differential equation in r, which is much easier to program and saves computational time. The derivation of the reduced form of k_7 requires a change of the order of integration, summarized as

$$\int_r^1 dr_1 \int_0^{r_1} dr_2 = \int_0^r dr_2 \int_{r_2}^1 dr_1 + \int_r^1 dr_2 \int_{r_2}^1 dr_1. \tag{36}$$

With these reductions, one can now deduce in a straightforward manner that the L-matrix must be symmetric. Namely, implementing Eqs. (33) and (34) into Eq. (32) it follows that $L_{21} = L_{12}$ and $L_{32} = L_{23}$. Finally, using the boundary conditions of $\psi(x, r)$ and the PB-equation (14) one can also show that $L_{31} = L_{13}$ and thus prove symmetry of the flux-force matrix. The final reduced form of the L-matrix can thus be written as

$$\begin{aligned}
L_{11} &= \frac{1}{8} \\
L_{22} &= 8c_v^2 k_7 + 4c_v \int_0^1 r \cosh\psi(r) dr \\
L_{33} &= -8c_v \int_0^1 r \left(\sinh\psi(r) \lambda_{\text{ref}}^2 (\psi(r) - \psi_{\text{wall}}) - \frac{1}{2}\cosh\psi(r) \right) dr \\
L_{21} &= L_{12} = c_v \int_0^1 (r - r^3) \cosh\psi(r) dr \\
L_{31} &= L_{13} = 4 \int_0^1 r \lambda_{\text{ref}}^2 (\psi(r) - \psi_{\text{wall}}) dr \\
L_{23} &= L_{32} = 8c_v \int_0^1 r \left(\cosh\psi(r) \lambda_{\text{ref}}^2 (\psi(r) - \psi_{\text{wall}}) - \frac{1}{2}\sinh\psi(r) \right) dr
\end{aligned} \tag{37}$$

where the analytic form of L_{22} is new due to the single k_7 integral presented in Eq. (35).

4 Onsager symmetry, the second law and change of basis

Symmetry for flux-force matrices, as just shown for Eq. (31), is generally known as Onsager symmetry, a phenomenon characteristic for systems that are near equilibrium, under the assumption that the equations of motion are reversible upon small time increments.

One property of a matrix L that has (Onsager) symmetry, is that it has a positive determinant. This property has its roots in the Second Law of Thermodynamics that states that the entropy production is non-negative during an irreversible process. We here define the dissipated power density P in a slice of the cylinder ($x \in [a, b]$) as the product of fluxes and conjugate driving forces (i.e., only the diagonal elements are used)

$$P = -\overline{u_x} \cdot \frac{\Delta p_{t,v}(x)}{b-a} - \overline{j_{\text{ions},x}} \cdot \frac{\Delta \mu_v(x)}{b-a} - \overline{j_{\text{charge},x}} \cdot \frac{\Delta \phi_v(x)}{b-a} \tag{38}$$

which is analogous to the definition in Ref. [11]. If we were to re-assign dimensions to this equation we would see that it is a power density with units of W/m^3. By the Second Law of Thermodynamics, this equation has to be positive as the process it describes is irreversible. Now, passing to the limit $a \to b$ we see that

$$P = \overline{u_x} \cdot \left(-\frac{\partial p_{t,v}}{\partial x} \right) + \overline{j_{\text{ions},x}} \cdot \left(-\frac{\partial \mu_v}{\partial x} \right) + \overline{j_{\text{charge},x}} \cdot \left(-\frac{\partial \phi_v}{\partial x} \right). \tag{39}$$

We observe that when we insert Eq. (32), we can write Eq. (39) as

$$\left(-\frac{\partial p_{t,v}}{\partial x}, -\frac{\partial \mu_v}{\partial x} - \frac{\partial \phi_v}{\partial x} \right) \cdot L \cdot \left(-\frac{\partial p_{t,v}}{\partial x}, -\frac{\partial \mu_v}{\partial x} - \frac{\partial \phi_v}{\partial x} \right)^t > 0 \tag{40}$$

which is a statement of positive definiteness of the matrix L, because it should hold for arbitrary driving forces.

In the last part of this section, we will analyze the flux-force matrix formalism more generally and will come to the conclusion that there are many possible (actually, an infinite number of) coupled sets of flux-force equations that are equivalent to the set in Eq. (32) in the sense that Onsager symmetry is preserved and the dissipation rate is described by the product of fluxes and conjugate forces. Gross and Osterle [2] already showed quite extensively the equivalence of Eq. (32) and a coupled set with $\overline{u_x}, \overline{j_{\text{diff},x}}, \overline{j_{\text{charge},x}}$ as fluxes and $-\partial_x p_{h,v}, -\partial_x \pi_v, -\partial_x \phi_v$ as driving forces. Here, differential flow is defined as

$$\boldsymbol{j}_{\text{diff}}(x,r) = \frac{\boldsymbol{j}_{\text{ions}}(x,r)}{2c_v(x)} - \boldsymbol{u}(x,r). \tag{41}$$

However, it is quite an arduous effort to verify the claims of Ref. [2], as they performed the change of coupled relations simultaneously with the reduction of the integrals in Eq. (32). Interestingly, we found that their specific claims can be formulated in terms of a much more general case, very similar to the one described by de Groot and Mazur [12] as we will outline next. Let $\boldsymbol{J}$ denote a set of fluxes in the x-direction and $\boldsymbol{X}$ a set of coupled thermodynamic forces, such as $\boldsymbol{J} = (\overline{u_x}, \overline{j_{\text{ions},x}}, \overline{j_{\text{charge},x}})$ and $\boldsymbol{X} = (-\partial_x p_{t,v}, -\partial_x \mu_v, -\partial_x \phi_v)$. Let $\boldsymbol{J'}$ and $\boldsymbol{X'}$ be another coupled set of fluxes and driving forces, so that we have the relations

$$\boldsymbol{J} = L \cdot \boldsymbol{X} \text{ and } \boldsymbol{J'} = L' \cdot \boldsymbol{X'} \tag{42}$$

and the dissipation rate can be written in this notation as

$$P = \boldsymbol{J} \cdot \boldsymbol{X} = \boldsymbol{X}^t \cdot L \cdot \boldsymbol{X}. \tag{43}$$

Let us also define the (invertible) linear maps $A : \boldsymbol{R}^3 \to \boldsymbol{R}^3$ and $B : \boldsymbol{R}^3 \to \boldsymbol{R}^3$ by the relations

$$\boldsymbol{J'} = A \cdot \boldsymbol{J} \text{ and } \boldsymbol{X'} = B \cdot \boldsymbol{X} \tag{44}$$

making them the projections that carry $\boldsymbol{J}$ onto $\boldsymbol{J'}$ and $\boldsymbol{X}$ onto $\boldsymbol{X'}$. In general one can easily deduce that the equation

$$L' = A \cdot L \cdot B^{-1} \tag{45}$$

describes the relation between the coupled flux-force equations. Assuming that these projections are non-trivial (thus invertible) one can quite easily prove that Onsager symmetry is conserved and that the dissipation rate remains invariant under the associated change of basis (for arbitrary $\boldsymbol{X} \in \boldsymbol{R}^3$) if

$$A^t = B^{-1}. \tag{46}$$

Indeed, if this relation is assumed to hold we observe

$$(L')^t = (A \cdot L \cdot B^{-1})^t = (B^{-1})^t \cdot L^t \cdot A^t = A \cdot L \cdot B^{-1} \tag{47}$$

and

$$P' = \boldsymbol{J'} \cdot \boldsymbol{X'} = A \cdot \boldsymbol{J} \cdot B \cdot \boldsymbol{X} = \boldsymbol{J} \cdot A^t \cdot B \cdot \boldsymbol{X} = \boldsymbol{J} \cdot \boldsymbol{X} = P \tag{48}$$

which we set out to show.

We note that if we work with $\boldsymbol{J'} = (\overline{u_x}, \overline{j_{\text{diff},x}}, \overline{j_{\text{charge},x}})$ and $\boldsymbol{X'} = (-\partial_x p_{h,v}, -\partial_x \pi_v, -\partial_x \phi_v)$ and our original sets, then A and B are given by

$$A = \begin{pmatrix} 1 & 0 & 0 \\ -1 & \frac{1}{2c_v} & 0 \\ 0 & 0 & 1 \end{pmatrix} \text{ and } B = \begin{pmatrix} 1 & 2c_v & 0 \\ 0 & 2c_v & 0 \\ 0 & 0 & 1 \end{pmatrix}. \tag{49}$$

It is now straightforward to verify that $A^t = B^{-1}$, thereby proving the claim of Gross and Osterle [2]. The matrix L' can be calculated directly using these expressions and Eq. (42) and was found to be in agreement with Eq. (22) in Ref. [2].

5 Full equations of motion and numerical results

Returning to our original flux-force matrix, it is possible to obtain full (x, r)-dependent expressions for the three fluxes by inserting Eq. (30) into Eqs. (23) and omitting the averaging step. Using Eq. (36) one can reduce these equations to the set

$$\begin{pmatrix} u_x(r) \\ j_{\text{ions},x}(r) \\ j_{\text{charge},x}(r) \end{pmatrix} = \begin{pmatrix} L'_{11} & L'_{12} & L'_{13} \\ L'_{21} & L'_{22} & L'_{23} \\ L'_{31} & L'_{32} & L'_{33} \end{pmatrix} \cdot \begin{pmatrix} -\frac{\partial p_{t,v}}{\partial x} \\ -\frac{\partial \mu_v}{\partial x} \\ -\frac{\partial \phi_v}{\partial x} \end{pmatrix} \tag{50}$$

where

$$\begin{aligned}
L'_{11} &= +\frac{1}{4}(1-r^2) \\
L'_{12} &= -2c_v \left(\ln r \int_0^r r_1 \cosh\psi(r_1) dr_1 + \int_0^r r_1 \ln r_1 \cosh\psi(r_1) dr_1 \right) \\
L'_{13} &= +2\lambda_{\text{ref}}^2 (\psi(r) - \psi_{\text{wall}}) \\
L'_{21} &= +\frac{1}{2} c_v (1-r^2) \cosh\psi(r) \\
L'_{22} &= -4c_v \cosh\psi(r) \left(c_v \left(\ln r \int_0^r r_1 \cosh\psi(r_1) dr_1 + \int_0^r r_1 \ln r_1 \cosh\psi(r_1) dr_1 \right) - \frac{1}{2} \right) \\
L'_{23} &= +4c_v \left(\cosh\psi(r) \lambda_{\text{ref}}^2 (\psi(r) - \psi_{\text{wall}}) - \frac{1}{2} \sinh\psi(r) \right) \\
L'_{31} &= -\frac{1}{2} c_v (1-r^2) \sinh\psi(r) \\
L'_{32} &= +4c_v \sinh\psi(r) \left(c_v \left(\ln r \int_0^r r_1 \cosh\psi(r_1) dr_1 \int_0^r r_1 \ln r_1 \cosh\psi(r_1) dr_1 \right) - \frac{1}{2} \right) \\
L'_{33} &= -4c_v \left(\sinh\psi(r) \lambda_{\text{ref}}^2 (\psi(r) - \psi_{\text{wall}}) - \frac{1}{2} \cosh\psi(r) \right).
\end{aligned} \tag{51}$$

Solving for these fluxes, considering the appropriate boundary conditions, yields a complete picture of the behavior of the ions in the cylindrical pore. The calculation is based on a pore placed between two electrolyte solutions with c_{ext}=500 and 10 mM salt concentration, thus $c_v(x=0) = 2.48$ and $c_v(x=1) = 0.0495$ where $c_{\text{ref}} = 202$ mM based on a pore radius of $R = 2$ nm, pore length of $L = 100$ μm, an average ion diffusion coefficient of $D = 2 \cdot 10^{-9}$ m^2/s, viscosity of $\mu = 1$ mPa.s, and temperature $T = 298$ K. The permittivity of water is $\varepsilon = 6.91 \cdot 10^{-10}$ F/m, $\lambda_{\text{ref}} = 0.377$, the thermal voltage is $\Psi_B = 25.7$ mV and surface charge is $\sigma = -10$ mC/m^2. We assume the two reservoirs to have the same hydrostatic pressure, thus $p_{h,v}(x=0) = p_{h,v}(x=1)$. We apply a current of $\overline{j_{\text{charge},x}} = 0.693$ which translates dimensionally to 230 A/m^2. Note that the virtual potential, ϕ_v, at the inlet and outlet $(x = 0, 1)$, is equal to the "real" potential just outside the pore (outside the EDL layer at the pore mouths). The same holds for the virtual salt concentration, c_v, and virtual total pressure, $p_{t,v}$, though the external concentration and pressure must be divided by c_{ref} (and by $R_g T$ for $p_{t,v}$) to correspond to c_v and $p_{t,v}$ at $x = 0$ and $x = 1$.

We evaluate the flux-force formalism (31) along the length of the pore (x-direction), to find the profiles of the virtual quantities $p_{t,v}(x), \mu_v(x)$ and $\phi_v(x)$ for averaged fluxes that are invariant through the pore, $\overline{u_x}$, $\overline{j_{\text{ions},x}}$ and $\overline{j_{\text{charge},x}}$. Finally, using the continuity equation (2), we can also solve for the radial components of the fluxes, as their axial component is known on every point of the grid, which reduces the continuity equation to a first order r-dependent differential equation, to generate streamline and vectorfield-plots for $\boldsymbol{u}$, $\boldsymbol{j}_{\text{ions}}$, and $\boldsymbol{j}_{\text{charge}}$.

For external salt concentrations of c_{ext}=500 mM (at the left-hand pore entrance, where $x = 0$) and c_{ext}=10 mM (at the right-hand side, $x = 1$), we can directly calculate the profiles of the radial contribution of the electrical potential $\psi(x, r)$, plotted in Fig. 2. Because the Debye length increases through the pore due to its reciprocal dependence on $c_v(x)$, we see that the radial potential $\psi(x, r)$ drops off faster (relatively) from the wall towards the pore axis at $x = 0$ (panel A) than at $x = 1$ (panel B). Also, the magnitude of $\psi(x, r)$ is much higher at $x = 1$ for c_{ext}=10 mM.

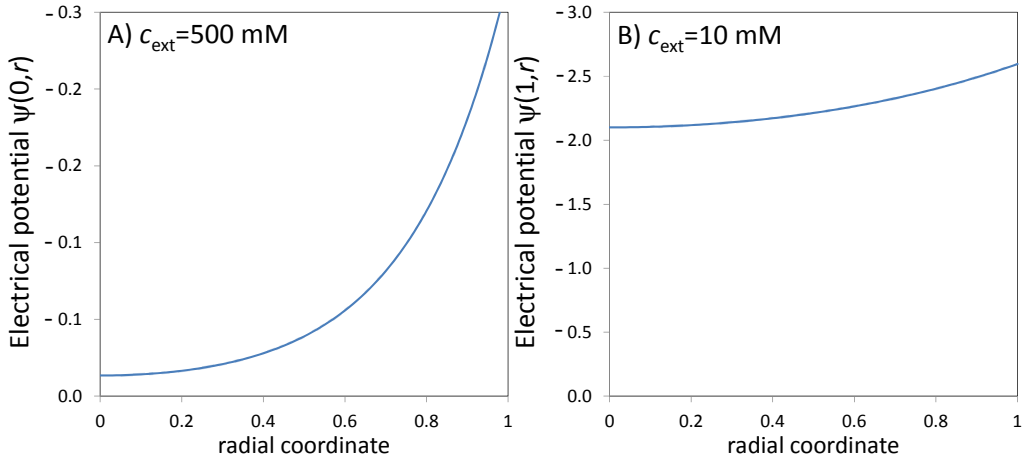

Figure 2: The electrical potential $\psi(0, r)$ and $\psi(1, r)$ at the two pore mouths as a function of the radial coordinate. At $x = 0$, the potential drops off more quickly (relatively) from the wall towards the pore axis as the result of a higher c_{ext}.

For the virtual quantity $c_v(x)$ (and thus $\mu_v(x) = \ln c_v(x)$ and $p_{t,v}(x)$) we find a gradual change from one end of the pore to the other [not shown]. However, for the virtual hydrostatic pressure $p_{h,v}(x)$ and virtual electrical potential $\phi_v(x)$, the behavior is more interesting, see Fig. 3. First of all, the hydrostatic pressure, though zero at both pore mouths, makes a steep excursion within the pore, reaching a maximum value of $p_{h,v} \sim 82$ kPa, corresponding to the osmotic pressure of a 17 mM salt solution. The electrical potential, $\phi_v(x)$, is virtually unchanging for most of the pore ($0 < x < 0.8$) before steeply increasing at the very end of the pore. Interestingly, $\phi_v(x)$ is slightly negative at the beginning of the pore before turning positive.

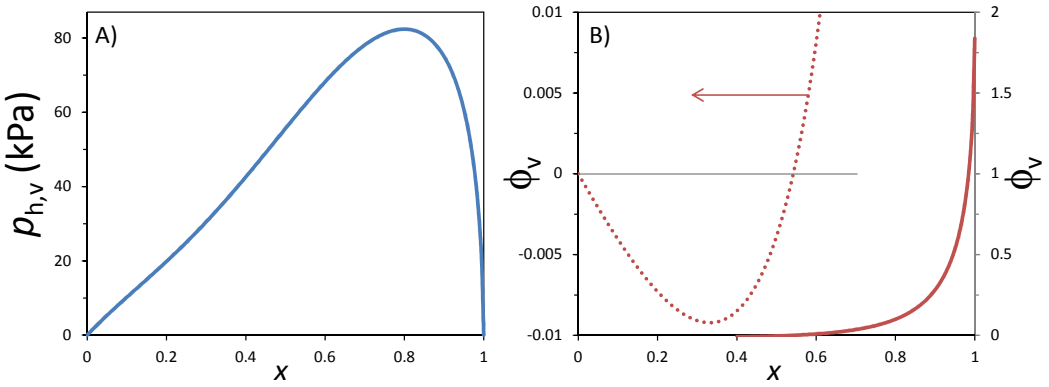

Figure 3: Plots of A) the virtual hydrostatic pressure $p_{h,v}(x)$, and B) virtual electrical potential, $\phi_v(x)$ over the length of the pore. In B) the dashed line gives an enlarged view of the potential profile for x <0.6.

Concerning the fluxes, the average flux of ions and velocity of the fluid are calculated as $\overline{j_{\text{ions},x}}$=4.63 and $\overline{u_x}$=-0.0247 for the chosen parameter set. This implies that the ions move to the right, while the water flows to the left, in agreement with the common notion of the solvent flowing to the side of lower total pressure (the side of higher salinity in case of equal hydrostatic pressure). For the profiles of the x-component of the fluxes across the pore, we find for the water velocity $u_x(r)$ a close-to parabolic shape (with no-slip at the wall), essentially constant through the pore, while $j_{\text{ions},x}(r)$ does not vary much with axial nor radial coordinate, from a value of ∼4.31 in the center, to ∼4.85 at the wall [not shown]. Thus note that the highest ion fluxes are found at the wall.

For the profile in ionic current, $j_{\text{charge},x}(r)$ we also find the highest value at the wall, $j_{\text{charge},x}(1) \sim 1.73$, but interestingly, in the center of the pore we find an inversion of ionic current. In particular, at $x = 0$, $j_{\text{charge},x}(r)$ is always positive, increasing from $j_{\text{charge},x}(0) = 0.30$ to $j_{\text{charge},x}(1) = 1.49$. However, at $x = 1$, $j_{\text{charge},x}(0)$ =-0.40 while $j_{\text{charge},x}(1)$=1.88. This change-over in $j_{\text{charge},x}(0)$ from positive at $x = 0$ to negative at $x = 1$, implies that there is a "surface" within the pore where the x-component of the ionic

current is zero. This is indeed shown to be the case in Fig. 4 where plots are presented for streamlines and local magnitudes in $\boldsymbol{j}_{\text{charge}}$. As Fig. 4 shows, even though the average ionic current is positive (directed to the right), there is a range of r-positions around the center axis where the ionic current enters the pore on the *right-hand* side, flowing to the left, before looping back and exiting the pore again on the right, but now closer to the wall.

In presenting streamline and vectorfield plots in Fig. 4, one might notice a paradox, as we assumed equilibrium in the r-direction, which should result in $j_{\text{charge},r} = 0$ for all x, r. This seems to clash with our calculation of $\boldsymbol{j}_{\text{charge}}$ by virtue of the continuity equation (2), which very clearly results in a vector field of $\boldsymbol{j}_{\text{charge}}(x, r)$ that has non-zero r-components. This paradox is solved by noticing that we normalized our x- and r-coordinates to a $[0, 1] \times [0, 1]$ square. To obtain the true magnitude of our vector components one has to multiply all r-components by R and all x-components by L. The latter is much larger and this justifies the claim that the r-component of $\boldsymbol{j}_{\text{charge}}(x, r)$ is almost 0.

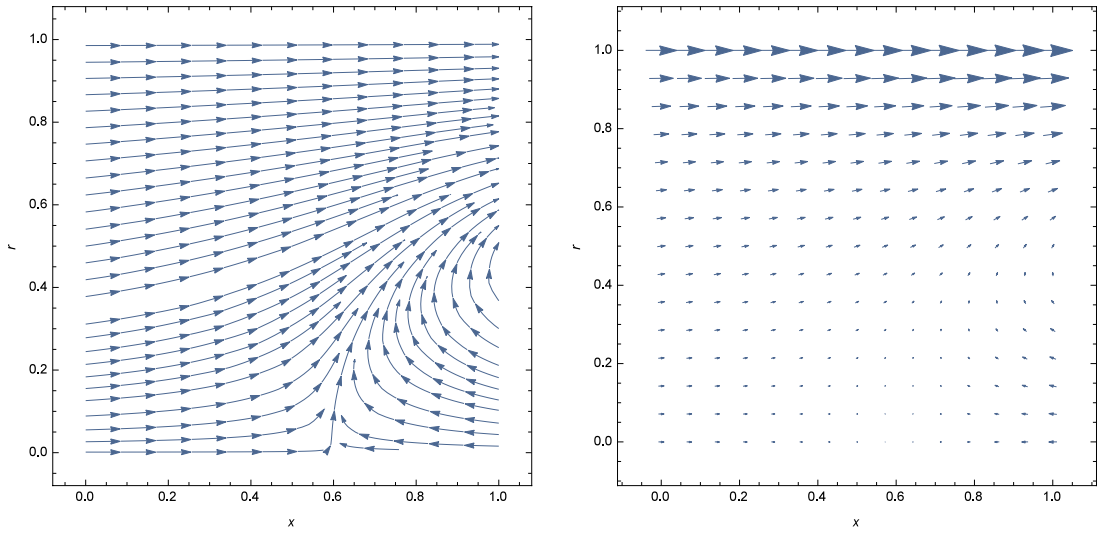

Figure 4: Streamline (left) and vectorfield (right) plots of the charge flux $\boldsymbol{j}_{\text{charge}}(x, r)$. The streamline plot clearly demonstrates the inversion of $\boldsymbol{j}_{\text{charge}}(x, r)$, while the vectorfield plot provides insight into the larger magnitude of the charge flux near the pore wall.

To our knowledge this is the first time that for a long an narrow charged pore, computations of the capillary pore model are made in the presence of an axial concentration gradient. Ref. [13] considered an axial concentration gradient but their method involved solving the NS-, NP- and PB-equations directly, for a system far from the "needle limit" of $L/R \to \infty$. Instead, the geometry considered was for a pore even wider than long (i.e., $L/R < 1$). In ref. [13] an inversion within the pore of one of the fluxes was observed, namely in $\boldsymbol{u}_x(x, r)$. Our analysis, therefore, provides a new perspective on the generality of this phenomenon. We hope that calculating the full vector fields $\boldsymbol{u}(x, r), \boldsymbol{j}_{\text{ions}}(x, r)$ and $\boldsymbol{j}_{\text{charge}}(x, r)$ via the formulation of averaged fluxes will prove useful to find other flux inversions as well.

Finally we show how our calculations can provide relevant information on the performance of an electrokinetic energy harvesting device based on a salt concentration difference. Here, we consider the single membrane pore as part of a membrane, placed in an overall electrical circuit. Because of the salt concentration difference across the membrane, ultimately power is delivered to a load R, see Fig. 1. In the remainder of this section, we will drop the overbar-sign, as well as subscript "x", to denote average, axial, fluxes.

In general we can define the efficiency of the generation of electrical energy at any point in the membrane as

$$\eta' = -\frac{j_{\text{charge}} \partial_x \phi_v}{j_{\text{ions}} \partial_x \mu_v + u \partial_x p_{t,v}}. \tag{52}$$

For a zero overall hydrostatic pressure, integrating over the entire pore length, Eq. (52) results for energy efficiency η in

$$\eta = -\frac{j_{\text{charge}} \Delta \phi_v}{j_{\text{ions}} \Delta \mu_v - u \Delta \pi_v} \tag{53}$$

noting that differences Δ are defined as conditions at "$x = 1$" minus at "$x = 0$". In Fig. 5 we plot

η versus the electrical power generated by a single nanopore (instead of plotting both versus current or voltage as in ref. [14]). These calculations are based on external salt concentrations of c_{ext}=100 and 10 mM, with all other parameter settings the same as before. The maximum in energy conversion efficiency of $\eta \sim 28\%$ is obtained for a current of $\sim$200 A/m^2 ($\Delta\phi_v \sim 31$ mV; salt transport efficiency $\vartheta = j_{\text{charge}}/j_{\text{ions}} \sim 63\%$). Around this optimum the fluid velocity, u, switches from normal osmosis (directed to the high-salinity side at lower currents), to anomalous osmosis at higher currents, where the fluid flows to the low-salinity side. In the present calculation, the fluid velocity is found to vary between u =-0.7 μm/s for open-circuit conditions (zero current, $\Delta\phi_v \sim 47$ mV) to u =+1.6 μm/s for electrical short-circuit ($\Delta\phi_v = 0$, current ~ 540 A/m^2).

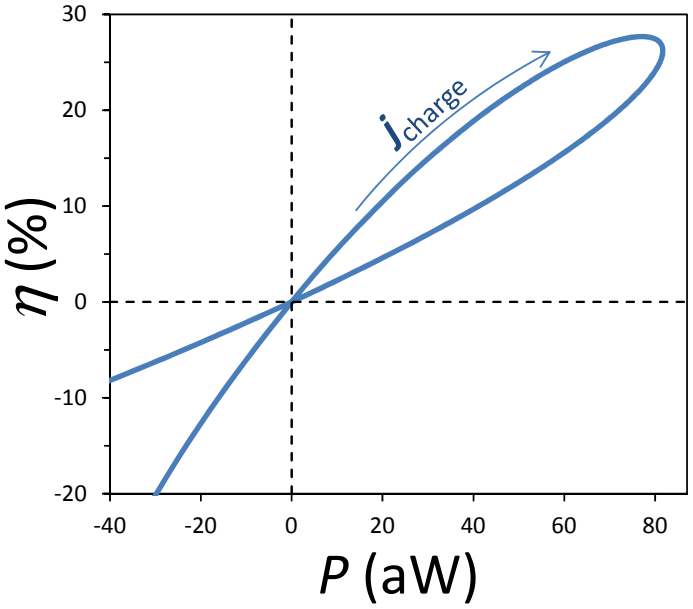

Figure 5: Plot of energy efficiency η against generated electrical power P by a single charged nanopore placed between two electrolytes of different salinity (c_{ext} =100 and 10 mM). The current increases in the direction of the arrow.

6 Conclusions

For the flux-force framework for ionic transport through charged capillaries we have revisited the work of Osterle and coworkers [2, 3] and discovered a single-integral expression for the coefficient k_7. We demonstrate how from one (Onsager-)symmetric flux-force framework other equivalent frameworks can be rigorously derived. We present numerical calculation results for pore subjected to two reservoirs with different salt concentrations, and show how in the presence of an overall concentration difference a "current loop" can develop at one of the pore ends. We present a plot of energy efficiency versus the electrical power generated by a single charged nanopore.

Acknowledgments

This work is part of the Delta-ITP consortium, a program of the Netherlands Organisation for Scientific Research (NWO) that is funded by the Dutch Ministry of Education, Culture, and Science (OCW). Part of this work was performed in the cooperation framework of Wetsus, European Centre of Excellence for Sustainable Water Technology (www.wetsus.eu). Wetsus is co-funded by the Dutch Ministry of Economic Affairs and Ministry of Infrastructure and Environment, the Province of Fryslân, and the Northern Netherlands Provinces.

References

[1] T. Teorell, *Progress in Biophysics and Biophysical Chemistry* **3** 305 (1953).

[2] R.J. Gross and J.F. Osterle, *J. Chem. Phys.* **49** 228 (1968).

[3] J.C. Fair and J.F. Osterle, *J. Chem. Phys.* **54** 3307 (1971).

[4] V. Sashidar and E. Ruckenstein, *J. Colloid Interface Sci.* **82** 439 (1981).

[5] X.L. Wang, T. Tsuru, S.-I. Nakao, and S. Kimura, *J. Membrane Sci.* **103** 117 (1995).

[6] F.H.J. van der Heyden, D.J. Bonthuis, D. Stein, C. Meyer, and C. Dekker, *Nano Lett.* **6** 2232 (2006).

[7] M.M. Hatlo, D. Panja, and R. van Roij, *Phys. Rev. Lett.* **107** 068101 (2012).

[8] B.D. Kang, H.J. Kim, M.G. Lee, and D.K. Kim, *Energy* **86** 525 (2015).

[9] M.B. Andersen, M. van Soestbergen, A. Mani, H. Bruus, P.M. Biesheuvel, and M.Z. Bazant, *Phys. Rev. Lett.* **109** 108301 (2012).

[10] R.J. Gross, *Membrane Transport Characteristics*, Dept. Mech. Eng., Carnegie Institute of Technology (1967).

[11] M.Z. Bazant, *Electrokinetic Energy Conversion*, Electrochemical Energy Systems, Lecture 31 (2011).

[12] S.R. de Groot and P. Mazur, *Non-equilibrium Thermodynamics*, North-Holland Publishing Company (1962).

[13] C.E. Wyman and M.D. Kostin, *J. Chem. Phys.* **59** 35 (1973).

[14] S. Porada, D. Weingarth, H.V.M. Hamelers, M. Bryjak, V. Presser, and P.M. Biesheuvel, *J. Mater. Chem. A* **2** 9313 (2014).